5-2022

# Assessing Manganese Concentrations in Groundwater Across the Shenandoah Valley, VA

Christopher Goldmann
*Trinity University*, cgoldman@trinity.edu

Follow this and additional works at: https://digitalcommons.trinity.edu/geo_honors

# ASSESSING MANGANESE CONCENTRATIONS IN GROUNDWATER ACROSS THE SHENANDOAH VALLEY, VA

Christopher Goldmann

A DEPARTMENT HONORS THESIS SUBMITTED TO THE
DEPARTMENT OF GEOSCIENCES AT TRINITY UNIVERSITY
IN PARTIAL FULFILLMENT OF THE REQUIREMENTS FOR GRADUATION WITH
DEPARTMENTAL HONORS

DATE \_\_\_\_\_April 29, 2022_____

\_\_\_Dr. Brady Ziegler_____         \_\_\_\_\_Dr. Benjamin Surpless_____
THESIS ADVISOR                          DEPARTMENT CHAIR

_____
Jennifer Henderson, AVPAA

**Student Agreement**

I grant Trinity University ("Institution"), my academic department ("Department"), and the Texas Digital Library ("TDL") the non-exclusive rights to copy, display, perform, distribute and publish the content I submit to this repository (hereafter called "Work") and to make the Work available in any format in perpetuity as part of a TDL, digital preservation program, Institution or Department repository communication or distribution effort.

I understand that once the Work is submitted, a bibliographic citation to the Work can remain visible in perpetuity, even if the Work is updated or removed.

I understand that the Work's copyright owner(s) will continue to own copyright outside these non-exclusive granted rights.

I warrant that:

  1) I am the copyright owner of the Work, or
  2) I am one of the copyright owners and have permission from the other owners to submit the Work, or
  3) My Institution or Department is the copyright owner and I have permission to submit the Work, or
  4) Another party is the copyright owner and I have permission to submit the Work.

Based on this, I further warrant to my knowledge:

  1) The Work does not infringe any copyright, patent, or trade secrets of any third party,
  2) The Work does not contain any libelous matter, nor invade the privacy of any person or third party, and
  3) That no right in the Work has been sold, mortgaged, or otherwise disposed of, and is free from all claims.

I agree to hold TDL, DPN, Institution, Department, and their agents harmless for any liability arising from any breach of the above warranties or any claim of intellectual property infringement arising from the exercise of these non-exclusive granted rights."


**I choose the following option for sharing my thesis (required):**

[**x**] Open Access (full-text discoverable via search engines)
[  ] Restricted to campus viewing only (allow access only on the Trinity University campus via digitalcommons.trinity.edu)

**I choose to append the following Creative Commons license (optional):**

# ASTRACT

Aqueous manganese ($Mn^{2+}$) in groundwater used for drinking water has adverse aesthetic effects at concentrations $\geq$ 50 ppb and adverse human health effects at concentrations $\geq$ 100 ppb. $Mn^{2+}$ in groundwater may have anthropogenic (mines, pesticide, gasoline) or geogenic (rocks and minerals) sources. Private drinking water wells are vulnerable to $Mn^{2+}$ contamination because their water quality is not routinely monitored. This study uses groundwater data from 1587 private wells in the Shenandoah Valley, VA to assess the spatial distribution of $Mn^{2+}$ in groundwater and identify possible $Mn^{2+}$ contamination mechanisms. Using geospatial and statistical analyses I found that samples collected near the valley center predominantly in shale host lithologies contained $Mn^{2+} \geq$ 50 ppb more frequently (26%) than sandstone (25%), metamorphic (13%), limestone (3%), dolostone (2%), igneous (0%), and black shale (0%) lithologies. Additionally, samples collected in closer proximity to surface water had higher $Mn^{2+}$ concentrations. Groundwater samples with elevated $Mn^{2+}$ ($\geq$ 100 ppb) occurred on average 206 m from surface water as opposed to 304 m on average for low $Mn^{2+}$ samples ($\leq$ 100 ppb). Our data suggest that elevated $Mn^{2+}$ in groundwater occurs near rivers at the valley center where old, anoxic groundwater upwells and reductively dissolves Mn oxides in soils and sediment. Overall, those who source drinking water from wells in the Shenandoah Valley should be cautious of consuming untreated water within shale lithologies.

# INTRODUCTION

Elevated concentrations of manganese (Mn) in drinking water can have a multitude of adverse human health effects and undesirable aesthetic consequences. Chronic exposure to aqueous manganese (Mn) concentrations ≥ 300 parts per billion (ppb) elicits a variety of negative health effects including reduced IQ, increased infant mortality and cancer rates, and increased risk of Parkinson's disease (Bjørklund et al., 2017; Bouchard et al., 2007; Bouchard et al., 2011; Hafeman et al., 2007; Khan et al., 2012; Langley et al., 2015; Sanders et al., 2014; Spangler and Spangler, 2009; Spangler and Reid, 2010). The Environmental Protection Agency (EPA) has established a lifetime chronic exposure maximum contaminant level (MCL) of 300 ppb (U.S. Environmental Protection Agency, 2004), though negative health effects have been documented with chronic exposure to $Mn^{2+}$ ≥ 100 ppb (Ljung and Vahter, 2007; Langley et al., 2015; Sanders et al., 2014). Additionally, the EPA has set a 1-day and 10-day health advisory (HA) for acute exposure to aqueous $Mn^{2+}$ at 1 mg/L and a secondary maximum contaminant level (SMCL) for aqueous $Mn^{2+}$ at 50 ppb to avoid bitter metallic tastes and staining (U.S. Environmental Protection Agency, 2004).

Mn can be introduced to groundwater through a variety of geogenic and anthropogenic mechanisms. Most commonly, high concentrations of dissolved organic carbon (DOC) in aquifer soils and sediments can stimulate microbial populations and rapidly deplete dissolved oxygen to generate a reducing environment, under which Mn(IV)-oxides are reductively dissolved to aqueous $Mn^{2+}$ (Di-Ruggiero and Gounot, 1990). This reaction is shown in Eq. 1, where $CH_2O$ represents generalized organic matter.

$$MnO_2 + 0.5CH_2O + 1.5H^+ \rightleftharpoons 0.5\ HCO_3^- + Mn^{2+} + H_2O \qquad \textbf{Eq. 1}$$
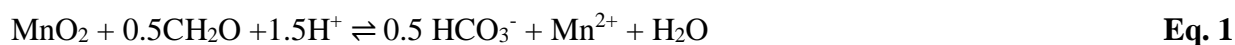
Thus, environments with shallow anoxic water tables, elevated DOC in host soils, and/or host lithologies containing organic matter (e.g., shale) often contain elevated aqueous $Mn^{2+}$.

Soil weathering may increase the quantity of Mn(IV)-oxides available for reductive dissolution. For example, in the Piedmont Plateau of North Carolina, chemical weathering of near-surface soil and saprolite dissolves primary Mn(II,III)-bearing minerals that precipitate as secondary Mn(III,IV)-oxides near the water table. Under reducing conditions, these secondary Mn oxides dissolve and mobilize $Mn^{2+}$ in groundwater (Gillispie et al., 2016).

Possible anthropogenic sources of Mn include, but are not necessarily limited to, Mn mines, pesticides, and gasoline. Mn ores were historically mined for the production of dry batteries, flint glass, steel, and gunpowder (Mendenhall and Monroe, 1942). Mines expose Mn oxides at the surface and accelerate weathering, thus soils in the proximity tend to be elevated in Mn oxides available for reductive dissolution and mobilization in groundwater recharge (Hue et al. 2001; Li et al. 2007). The Mn-containing chemicals Maneb® and Mancozeb® are commonly applied in orchards as a fungicide. Excessive application of these fungicides can lead to runoff, resulting in elevated concentrations of Mn in soils and/or groundwater (Semu and Singh, 1995). Lastly, when lead was banned by the Clean Air Act in 1996 as an additive to gasoline, it was replaced by the Mn-bearing molecule methylcyclopentadienyl manganese tricarbonyl (MMT) in an effort to reduce engine knocking and boost octane ratings. Along major roadways, Mn accumulates in adjacent soils from engine exhaust and is potentially introduced into aquifers via runoff (Lytle et al., 1995).

The study area for this research is the Shenandoah Valley, Virginia, where at least 36% of the population uses private wells for drinking water (Virginia State Water Resources Plan, 2015; U.S. Census Bureau, 2019). While regular testing and treatment of public water supplies is required by U.S. law, monitoring private supplies is optional and services are provided by the Virginia Household Water Quality Project (VAHWQP) upon request. The valley falls within the

Valley and Ridge Province, bordered by the Blue Ridge Province to the east and the Appalachian Plateaus Province to the west. The Valley and Ridge Province is geologically complex, with generalized host lithologies including shale, black shale, dolostone, limestone, sandstone, igneous, and metamorphic facies (USGS 2003, see Table 1). Many of the province's geologic units were deposited in a continental shelf environment during the Ordovician, prior to a series of orogenies that formed the Appalachians beginning with the Taconic Orogeny (ended 440 Myr) that folded and fractured sedimentary units (Wehr, 1985). Uplift and erosion created modern-day Appalachia, where durable sandstone tends to form cliffs and areas of high elevation while weaker shales and limestones form the valleys and river bottoms.

The Shenandoah Valley is a combination of multiple watersheds centered on the Shenandoah River. Groundwater flows anisotropically along fractures within bedding planes, which generally strike N. 30° E (Yager et al., 2009). Groundwater recharge occurs throughout the valley via bedrock fractures, while discharge is confined to springs along river channels and the headwaters of many tributaries. General groundwater flow is from topographic highs on the valley's periphery to the Shenandoah River at the valley's center; thus, groundwater ages generally increase from the margins of the valley to the center. However, localized areas with short recharge-discharge paths and relatively young groundwater ages exist in the valley (Yager et al., 2009).

The objective of this study was to isolate $Mn^{2+}$ groundwater contamination mechanisms specific to the Shenandoah Valley. By identifying variables associated with elevated $Mn^{2+}$ and identifying the primary mechanism by which $Mn^{2+}$ enters groundwater, the valley's population reliant on private drinking wells can avoid many of the adverse health and aesthetic effects associated with elevated $Mn^{2+}$ concentrations in drinking water.

# METHODS

## Groundwater collection and analyses

This study utilizes well water data from VAHWQP and the United States Geological Survey (USGS) National Water Information System (NWIS). The VAHWQP dataset contains samples collected at private residences between 2009 and 2019. Samples were collected from the tap inside homes, guesthouses, and barns under a single address. During sample collection, both a "first draw" (obtained after a stagnation period in plumbing, usually overnight) and "flushed" (obtained after five minutes of continuous running tap) were collected: this study exclusively uses data from the "flushed" samples. Samples were filtered through a 0.2 μm filter and analyzed for $NO_3^-$ and $F^-$ using ion chromatography, while inductively coupled mass spectrometry (ICP-MS) was used to measure all other analytes (Na, Mg, Al, Si, P, $SO_4$, K, Ca, V, Cr, Fe, Mn, Co, Ni, Cu, Zn, As, Mo, Ag, Cd, Sn, Pb, Cl, Ti, Se, Sr, Ba, and U). In congruence with the testing of private water supplies, property owners answered questionnaires; topics addressed in the questionnaire included (but were not limited to) whether a water treatment system was present, plumbing construction materials, noticeable aesthetic deficiencies of water, proximity of the property to environmental hazards such as landfills, and whether any member of the household had been sick in the past 30 days.

Data from the USGS NWIS were compiled and reported by McMahon et al. (2018). NWIS data were collected between 1988 and 2017; all samples were collected directly from wells rather than household taps and filtered with a 0.45 μm filter, preserved with nitric acid and analyzed with ICP-MS. Data from VAHWQP and NWIS were combined into a single dataset, resulting in 1587

5

unique sampling locations and 1906 individual samples. Thus, 319 samples were collected at duplicate locations at a different point in time.

**Geospatial analyses**

The combined dataset was brought into ArcGIS Pro 2.8.3 for geospatial analysis. Additional publically available data used in this study are summarized in Table 2. Briefly, surface water (streams/rivers) data were compiled as a shapefile by the Virginia Department of Environmental Quality. Geologic structure (including faults, dikes, and sills) and lithology within the Shenandoah Valley were developed by USGS. It is assumed that surface lithology evinced by the geologic map reflects underlying aquifer lithology. Historic Mn mines within the Shenandoah Valley are sourced from the Bureau of Land Management (BLM), which offers data on mine locations, years of operation, and commodity minerals. A few orchards in the valley were identified based on VAHWQP questionnaire responses and plotted in ArcGIS to examine potential effects of fungicide application on groundwater $Mn^{2+}$ concentrations in the vicinity.

Soil chemistry data including Mn in the top five cm, A horizon, and C horizon are derived from a nationwide USGS survey conducted between 2007 and 2013. A ratio of the Mn concentration in top soil to Mn concentration in the C horizon (TOP/BOT ratio) for each soil sample point was calculated (Eq. 2):

$$\frac{TOP}{BOT} = \frac{[Mn\ (ppb)\ in\ top\ 5\ cm]}{[Mn\ (ppb)\ in\ C\ horizon]} \qquad \textbf{Eq. 2}$$

Next, the resulting TOP/BOT values were kriged to create a continuous TOP/BOT raster surface and clipped to the Shenandoah Valley. TOP/BOT values were operationally defined as low (<2), medium, (2 to 4), and high (>4). Higher TOP/BOT values are the result of higher Mn

concentrations in the top soil than the materials from which it is derived and can be used as a proxy

for anthropogenic inputs (pesticide application and gasoline).

**Table 1:** Geospatial Supplementary Information

| Data Layer | Compiling organization | Data source |
|---|---|---|
| Groundwater chemistry ($NO_3$, F, Na, Mg, Al, Si, P, $SO_4$, K, Ca, V, Cr, Fe, Mn, Co, Ni, Cu, Zn, As, Mo, Ag, Cd, Sn, Pb, Cl, Ti, Se, Sr, Ba, U) | VAHWQP, Virginia Tech<br><br>USGS NWIS | Erin Ling, *personal communication*<br><br>McMahon et al. (2018) |
| Surface water | Virginia Department of Environmental Quality | https://geohub-vadeq.hub.arcgis.com/datasets/e248a73e04b2458f9711ddc2ffc0857e_181/explore?location=37.594044%2C-81.154412%2C13.60 |
| Geologic structures | USGS | https://pubs.usgs.gov/of/2005/1325/ |
| Generalized lithology | USGS | https://mrdata.usgs.gov/geology/state/state.php?state=VA |
| Mines | Bureau of Land Management | https://thediggings.com/ |
| Orchards | Interpreted from VAHWQP questionnaire | Erin Ling, *personal communication* |
| Roadways | Virginia Department of Transportation | https://catalog.data.gov/dataset/tiger-line-shapefile-2015-state-virginia-primary-and-secondary-roads-state-based-shapefile |
| Soil chemistry | USGS | https://pubs.usgs.gov/sir/2017/5118/sir20175118_element.php?el=25 |
| DEM | USGS: The National Map | https://apps.nationalmap.gov/downloader/#/ |

The shortest linear distance between each groundwater sample location and surface water, geologic structure, and mines was calculated using the Near tool. This facilitated an assessment of spatial relationships between $Mn^{2+}$ concentrations in groundwater and features that may serve as an $Mn^{2+}$ input or contribute to reducing conditions and subsequent mobilization of aqueous $Mn^{2+}$.

A slope map for the valley was generated using the Slope tool and a 30 x 30 m resolution digital elevation model from The National Map managed by USGS (Table 1). To obtain this, 12 individual 1° x 1° quadrangles were compiled and geospatially referenced to create a large quadrangle of elevation data from which the data was clipped to an outline of the Shenandoah Valley.

**Statistical analyses**

*Data processing*

Multivariate statistical analyses can be useful for large chemical databases to elucidate patterns that inform geochemical mechanisms and processes occurring in a given system (Reimann, 2008). Therefore, the combined dataset from the VAHWQP and NWIS was passed through a hierarchical cluster analysis (HCA) and principle component analysis (PCA) in an attempt to tease out processes impacting water chemistry in the Shenandoah Valley. Because multivariate statistical methods require complete paired chemistry for each sample being considered, every analyte for every sample is required to have a reported value. However, some analytes only had reported values for a limited number of samples. For example, Cl was reported for only 985 of 1906 total samples. Meanwhile, some samples had reported values for only a fraction of analytes. Therefore, the dataset needed to be cropped in order to get a sample set with complete analyte data.

To crop the dataset, samples were removed if they lacked a reported value for Al, Si, P, V, Cr, Ni, Zn, As, Mo, Ag, Cd, Sn, and Pb. This cropped the dataset from 1906 samples with 31 analytes to 1488 samples with 31 analytes. However, some of these 1488 samples also lacked reported values for Cl, Ti, Se, Sr, Ba, and U. Two approaches were used to account for these missing values, as observed in Figure 1. First, samples without reported values for Cl, Ti, Se, Sr, Ba, and U were removed. This approach resulted in fewer overall samples (n = 985), with the reported values for all 31 analytes. For an alternate approach, rather than removing additional samples from the cropped dataset (1488 samples with 31 analytes), Cl, Ti, Se, Sr, Ba, and U were removed altogether, resulting in 1488 samples with 25 analytes. Hierarchical cluster analyses and principle component analyses were then performed on both datasets.
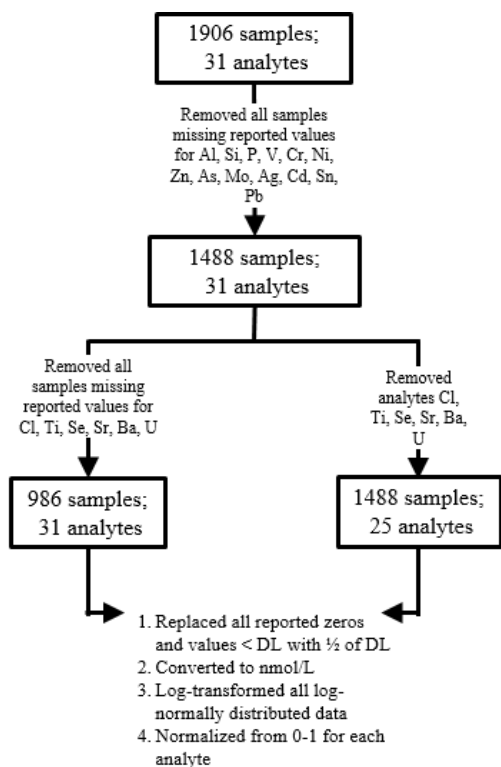


**Figure 1:** Flowchart of two alternate data filtering approaches prior to generating a HCA and PCA. Either the maximum number of samples was preserved (1488 samples across 25 analytes) or the maximum number of analytes was preserved (986 samples across 31 analytes).

Several analytes for several samples in the combined dataset contained reported values of zero and values less than the respective analyte detection limit. Because a concentration of "zero" and values less than the analytical detection limit bear little meaning, all values less than the detection limit for the analytical method for each respective analyte were replaced with half the detection limit (Reimann, 2008) (D.L. for $NO_3^-$ and $F^-$ was 0.1 mg/L, and the D.L for all other analytes was 1 μg/L). Concentrations were then converted to nmol/L based on each analyte's respective molar mass.

Multivariate statistical methods require normally distributed data, so each analyte was tested for normality using the Shapiro-Wilk test (Shapiro and Wilk, 1965). Of all the analytes, the p-value was $> 0.05$ for Si only, meaning that it was normally distributed while all other analytes were non-normally distributed. An inspection of the non-normally distributed analytes revealed a log-normal distribution, common for environmental samples. Thus values were log-transformed (with the exception of Si) to create a normal distribution for each analyte.

The normally distributed data were then scaled from zero to one for each analyte using the following approach (Eq. 3),

$$z_{i,j} = \frac{C_{i,j} - C_{min,j}}{C_{max,j} - C_{min,j}} \qquad\qquad \textbf{Eq. 3}$$

where $z$ is the scaled value from zero to one for sample $i$ and analyte $j$, $C_{i,j}$ is the normalized concentration for sample $i$ and analyte $j$, and $C_{min}$ and $C_{max}$ are the minimum and maximum normalized concentrations from all samples for analyte $j$, respectively.

*Hierarchical cluster analysis*

Hierarchical variable clustering was calculated using an algorithm that groups elements into clusters with the greatest similarity by minimizing the Aitchison distance between individual sample data (Kaufman and Rousseeuw, 1990) (all $z_{i,j}$ from Eq. 3). The algorithm then continues to

cluster more dissimilar clusters while minimizing Aitchison distance until all clusters are combined. Thus, clusters with the most similarity have the shortest Aitchison distance and are combined at the lowest height. As clusters become more dissimilar, the Atchison distance, and thus height, of the clusters increases.

*Principle component analysis*

Principle component analysis (PCA) is a dimension reduction method of multivariate data that aims to identify trends and variation in the data by reducing it to dimensionless latent variables (principle components) that account for the maximum variance in the multivariate dataset (Hotelling, 1933). The amount of variance in the data set that is explained decreases with each additional principle component.

PCA output generally is presented as a two-dimensional biplot that compares principal component one (x-axis) (PC1) vs principal component two (y-axis) (PC2), which explain the most and second-most variance in the data, respectively. Points, known as scores, plot the values of principal component one and principal component two for each sample. Vectors move away from the origin (which represents the geometric mean). The length of a variable's vector indicates the amount of control that variable exerts on the principal component in the vector's direction. Vectors that point in the same direction along a principal component axis are closely related, whereas vectors that point in the opposite direction along a principal component axis are inversely related, but still controlled by that same principal component. For example, if a principal component reflected redox state, one could expect dissolved $Fe^{2+}$ and $Mn^{2+}$ vectors to point in the same direction along the principal component axis and point in the opposite direction of dissolved oxygen.

# RESULTS

**Groundwater chemistry**

Summary statistics are presented in Table 2. They include quartiles, arithmetic means, and geometric means characterized by lithology to evaluate how $Mn^{2+}$ concentrations varied in different geologic materials in the Shenandoah Valley. Overall $Mn^{2+}$ concentrations in all 1906 samples range from <1 ppb (below the detection limit) to 7100 ppb. The arithmetic mean for all samples is 33.9 ppb while the geometric mean is 0.85 ppb, demonstrating a great abundance of low concentrations that is typical of environmental data. This disproportionate abundance of low concentrations is due to the log-normal distribution of $Mn^{2+}$ concentrations. Compared to other lithologies (black shale, dolostone, igneous, limestone, and metamorphic), shale and sandstone had higher $Mn^{2+}$ values for 25th percentile, 50th percentile, 75th percentile, arithmetic mean, and geometric mean. For example, the geometric mean $Mn^{2+}$ concentration (ppb) for sandstone and shale was 7.1 and 5.5 respectively, while the geometric mean for all samples (regardless of lithology) was 0.85. Several elevated $Mn^{2+}$ samples occurred in sandstone and shale, causing comparatively high geometric means in these lithologies.

**Table 2**: Summary statistics of groundwater $Mn^{2+}$ concentrations by various lithologies. Units are in ppb. Summary statistics for igneous aquifers were excluded because only four samples were characterized as igneous.

| Lithology | $Mn^{2+}$ Concentration (ppb) | | | | |
| | 25th percentile | 50th percentile | 75th percentile | Arithmetic mean | Geometric mean |
|---|---|---|---|---|---|
| Black shale | < 1 | < 1 | 3.1 | 3.6 | 0.7 |
| Dolostone | < 1 | < 1 | 1.0 | 7.2 | 0.3 |
| Limestone | < 1 | < 1 | 1.8 | 28.5 | 0.5 |
| Metamorphic | < 1 | 1.8 | 12.3 | 47.0 | 2.2 |
| Sandstone | 1.1 | 4.0 | 36.6 | 62.8 | 7.1 |
| Shale | < 1 | 2.7 | 57.8 | 97.1 | 5.5 |
| Overall | <1 | <1 | 3 | 33.9 | 0.85 |

The percentage of samples in exceedance of aesthetic and health benchmarks help inform the frequency and magnitude of $Mn^{2+}$ concentrations in the Shenandoah Valley. Only 10 samples exceeded the EPA 1 and 10-day health advisory limit of 1000 ppb, 60 samples exceeded the lifetime chronic exposure health advisory limit of 300 ppb, and 148 samples exceeded the SMCL of 50 ppb. Groundwater samples collected in shale and sandstone lithologies are generally higher in Mn. Additionally, a higher percentage of samples taken in shale and sandstone exceeded MCL, SMCL, and HA thresholds. For example, approximately 25% of all samples taken in sandstone and shale exceeded the aesthetic benchmark of 50 ppb, while only 8% of all samples (regardless of lithology) exceeded 50 ppb.

**Table 3:** Percentage of wells in exceedance of health or aesthetic benchmarks (SMCL, MCL, and HA) characterized by various lithologies.

| | % of wells in exceedance of: | | |
|---|---|---|---|
| Lithology | 50 ppb | 300 ppb | 1000 ppb |
| Black shale (n = 8) | 0 | 0 | 0 |
| Dolostone (n = 757) | 2 | 1 | 0 |
| Igneous (n = 4) | 0 | 0 | 0 |
| Limestone (n = 584) | 3 | 2 | 1 |
| Metamorphic (n = 210) | 13 | 6 | 0 |
| Sandstone (n = 16) | 25 | 6 | 0 |
| Shale (n = 326) | 26 | 10 | 2 |
| Overall (n = 1906) | 8 | 3 | 0.5 |

Bivariate plots were made from the 1906 samples to compare $Mn^{2+}$ versus depth and the 30 other chemical analytes reported in the combined VAHWQP and NWIS database. If a value was not reported for the comparison variable for a given sample, that sample was omitted from the bivariate analysis for that variable. Of the variables evaluated, a noteworthy relationship (e.g., correlation, anti-correlation, or lack of hypothesized correlation) with $Mn^{2+}$ was observed for one or more lithologies for the following variables: well depth, $Ca^{2+}$, $Mg^{2+}$, $Fe^{2+}$, $SO_4^{2-}$, $Co^{2+}$, and As

(Figure 2). In shale lithologies, $Mn^{2+}$ concentrations are low in samples close to the surface but dramatically increase at a depth of around 20 m. Below this depth, $Mn^{2+}$ concentrations generally decrease deeper into the aquifer: no $Mn^{2+}$ exceeding the MCL (>300 ppb) is observed deeper than ~150 m below the land surface.
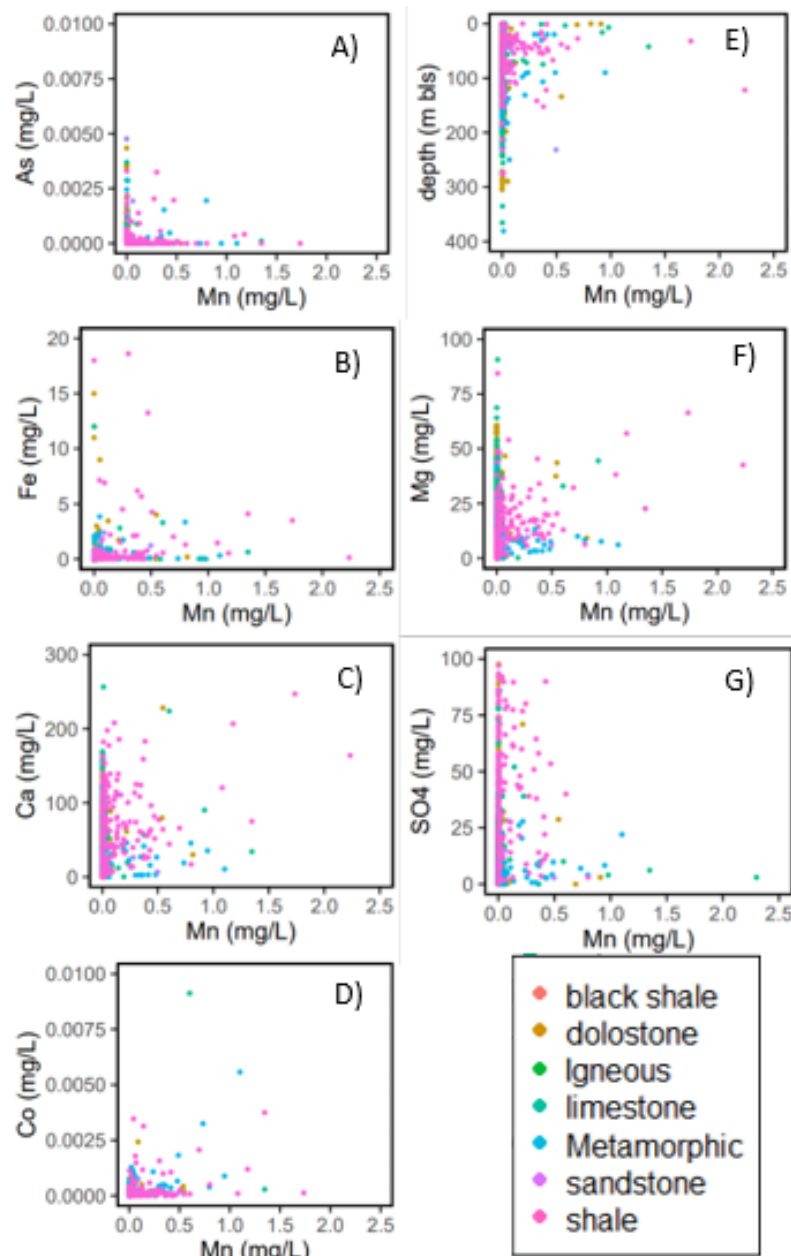


**Figure 2:** Groundwater analyte relationship scatterplots with $Mn^{2+}$ x As (A), $Mn^{2+}$ x $Fe^{2+}$ (B), $Mn^{2+}$ x $Ca^{2+}$ (C), $Mn^{2+}$ x $Co^{2+}$ (D), $Mn^{2+}$ x depth (E), $Mn^{2+}$ x $Mg^{2+}$ (F), and $Mn^{2+}$ x $SO_4^{2-}$ (G). All samples colorized by host lithology.

Generally, there is a positive correlation between $Mn^{2+}$ and $Ca^{2+}$: this correlation is strongest in shale (r = 0.750). A similar positive correlation is observed between $Mn^{2+}$ and $Mg^{2+}$, especially in shale (r = 0.767) and black shale (r = 0.548). A less pronounced positive correlation is observed between $Mn^{2+}$ and $Fe^{2+}$: several lithologies (limestone, metamorphic, and sandstone) exhibit a weak positive correlation (r < 0.4) while it is strongest in dolostone (r = 0.698), which is notable given the large sample size for dolostone (n = 757). Samples are typically high for either $Mn^{2+}$ or $SO_4^{2-}$ concentrations, but not both simultaneously, leading to overall low correlation coefficients. However, $SO_4^{2-}$ concentrations can be quite high, especially in shale lithologies. $Mn^{2+}$ and $Co^{2+}$ exhibit a positive correlation across all lithologies with the exception of black shale. The correlation is strongest in metamorphic lithologies (r = 0.695). Typically, samples were elevated in either $Mn^{2+}$ or As, but not both simultaneously. However, an exception to this trend occurred in shales, which had a relatively strong positive correlation between $Mn^{2+}$ and As (r = 0.753).

**Table 4:** Correlation coefficients for various parameters with $Mn^{2+}$ concentrations (ppb) in different lithologies

| | | correlation with coefficient (r) with $Mn^{2+}$ (ppb) | | | | | |
|---|---|---|---|---|---|---|---|
| Lithology | depth | $Ca^{2+}$ | $Mg^{2+}$ | $Fe^{2+}$ | $SO_4^{2-}$ | $Co^{2+}$ | As |
| Black shale | -0.025 | 0.078 | 0.548 | -0.003 | -0.337 | -0.198 | -0.306 |
| Dolostone | -0.093 | 0.120 | 0.051 | 0.698 | 0.094 | 0.224 | -0.025 |
| Igneous* | -0.481 | 0.412 | 0.382 | 0.057 | -0.682 | 0.661 | 0.474 |
| Limestone | -0.096 | 0.073 | 0.102 | 0.270 | 0.013 | 0.404 | -0.007 |
| Metamorphic | -0.105 | 0.120 | 0.024 | 0.228 | 0.005 | 0.695 | 0.152 |
| Sandstone | 0.978 | -0.197 | 0.016 | 0.358 | 0.318 | 0.213 | -0.155 |
| Shale | -0.075 | 0.750 | 0.767 | 0.072 | 0.260 | 0.259 | 0.753 |

*Igneous lithologies only contained four samples.

**Geospatial Relationships**

The spatial distributions of $Mn^{2+}$ concentrations in groundwater is depicted in Figure 3. The majority of elevated $Mn^{2+}$ samples (>100 ppb) occur in the northern part of the valley and near the

valley's center. Elevated $Mn^{2+}$ samples occur in curvilinear clusters, and isolated elevated $Mn^{2+}$ samples surrounded by low $Mn^{2+}$ rarely occur. Conversely, samples near the valley's southern end and along the eastern and western margins are comparatively low in Mn.
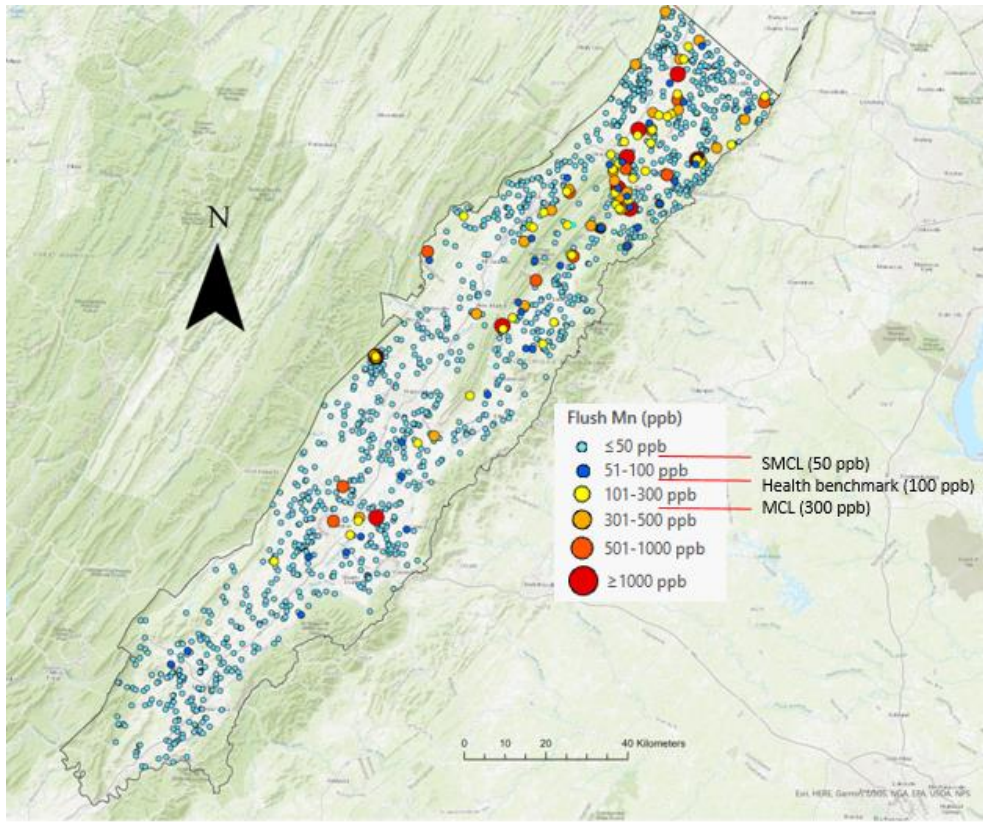


**Figure 3:** Spatial distribution of groundwater $Mn^{2+}$ concentrations in the Shenandoah Valley.

In Figure 3, $Mn^{2+}$ concentrations are projected with a potential explanatory variable: surface water, host lithology, geologic structure (faults, dikes, and sills), TOP/BOT ratio, slopes, and anthropogenic inputs (roads, orchards, and historic Mn mines). Generally, groundwater with elevated $Mn^{2+}$ concentrations (>100 ppb) tend to occur closer to surface water (Figure 3A). While the average distance of elevated $Mn^{2+}$ (>100 ppb) samples from surface water was 206 m, the average distance of all low $Mn^{2+}$ samples (<100 ppb) is significantly farther at 304 m. In particular, elevated $Mn^{2+}$ in groundwater often occurred near the headwaters of tributary streams/rivers.
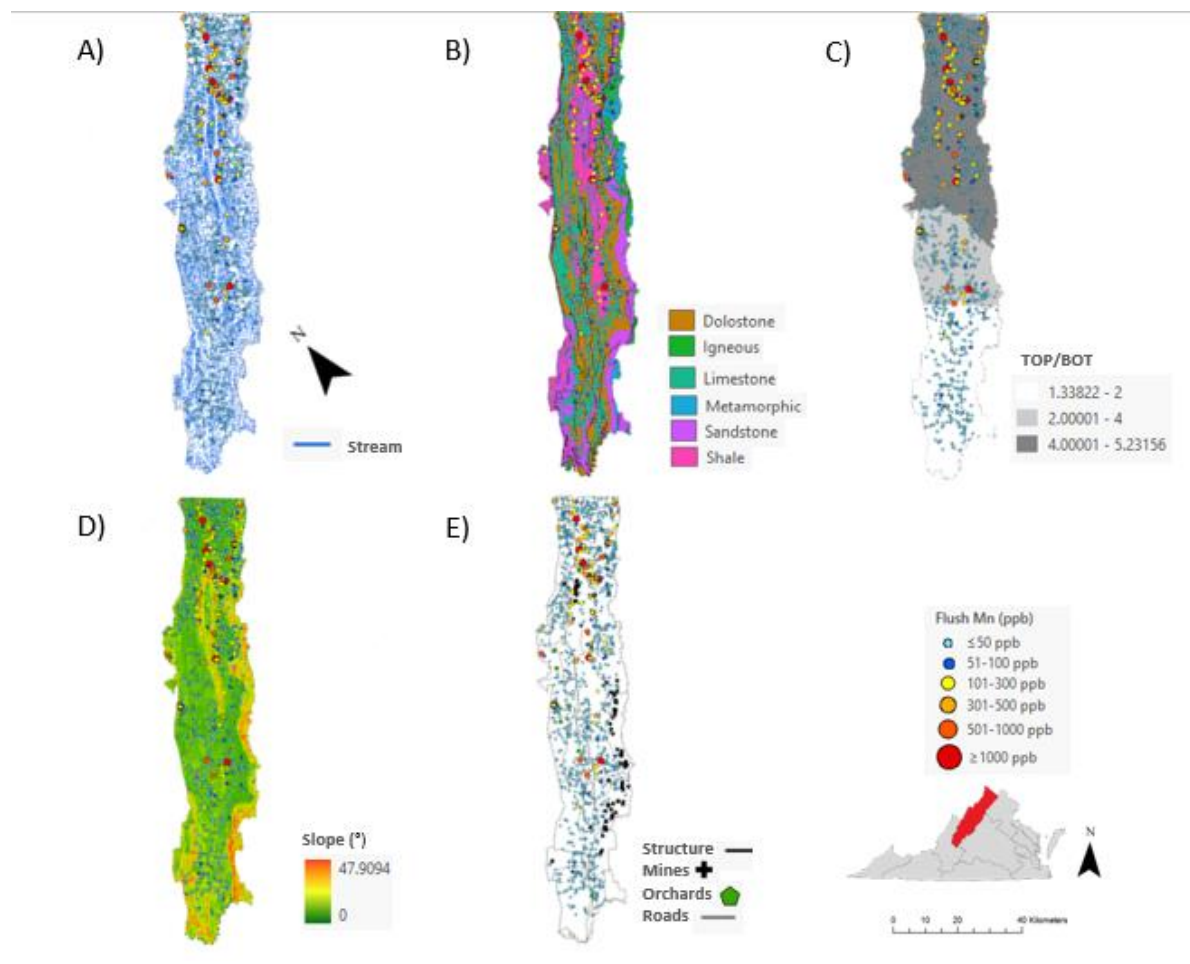
**Figure 4** Shenandoah Valley, VA maps with $Mn^{2+}$ concentrations and surface water (A), host geology (B), soil Mn TOP/BOT ratios (C), slope (D), and other potential contributing factors (E).

In Figure 4, $Mn^{2+}$ concentrations are projected with potential explanatory variables: surface water, host lithology, geologic structure (faults, dikes, and sills), TOP/BOT ratio, slopes, and anthropogenic inputs (roads, orchards, and historic Mn mines). Generally, groundwater with elevated $Mn^{2+}$ concentrations (>100 ppb) tend to occur closer to surface water (Figure 4A). While the average distance of elevated $Mn^{2+}$ (>100 ppb) samples from surface water was 206 m, the average distance of all low $Mn^{2+}$ samples (<100 ppb) is significantly farther at 304 m. In particular, elevated $Mn^{2+}$ in groundwater often occurred near the headwaters of tributary streams/rivers.

Aquifer lithology also appears to carry important implications for groundwater $Mn^{2+}$ concentrations (Figure 4B). Siliciclastic sedimentary lithologies (shales and sandstones) had the

highest average $Mn^{2+}$ concentrations, with a majority of elevated $Mn^{2+}$ samples underlain by the Martinsburg Formation. This predominantly shale formation underlies the vast majority of elevated $Mn^{2+}$ samples in the northern part of the valley as well as a few samples toward the unit's southern extent. However, a few elevated $Mn^{2+}$ samples occur in carbonate lithologies throughout the valley: this typically occurs near a boundary between carbonate and shale lithologies, thus shales are still in close proximity to these outlier samples.

Figure 4C displays groundwater data with a kriged TOP/BOT surface. A general trend of graded TOP/BOT values is observed, where values are low in the southern part of the valley, medium in the mid-latitudes of the valley, high in the north. While $Mn^{2+}$ concentrations in the C horizon are fairly constant throughout the valley, topsoil Mn concentrations gradually increase toward the north, thus causing the observed trend of increasing TOP/BOT values.

Figure 4D displays groundwater data with a slope map. Elevated groundwater $Mn^{2+}$ samples typically occur in areas of shallow slopes, though nearby areas of steeper slopes. This suggests elevated $Mn^{2+}$ in groundwater occur in the relatively flat floodplain nearby steeper river channels. Additionally, slopes are steepest in sandstone lithologies.

Figure 4E displays groundwater data with potential anthropogenic Mn inputs: roads, orchards, and historic Mn mines. Road construction regulations limit maximum percent grade to 6-7%, thus roads generally follow paths of low slope in the valley. Historic mines are concentrated along ridges along the southwestern margin of the valley as well as the northern end of the Massanutten Mountain Range in the northern region of the valley. While these historic mines reflect the presence of Mn ores, their existence does not seem to influence groundwater $Mn^{2+}$ concentrations in the vicinity. Orchards are sparsely distributed near the valley's western margin: given the lack

of orchards in proximity to samples with elevated Mn, their existence does not seem to influence groundwater $Mn^{2+}$ concentrations in the vicinity.
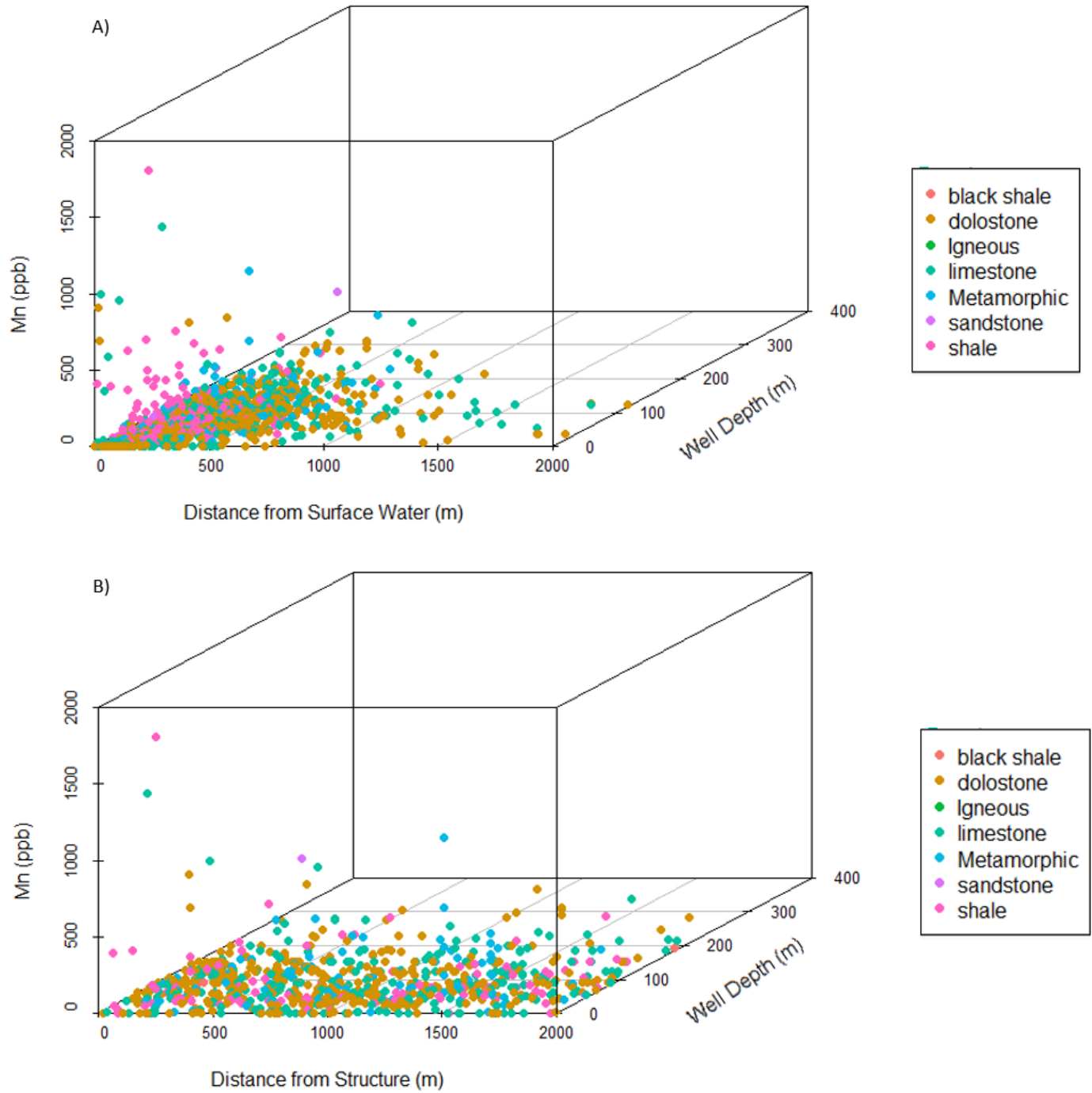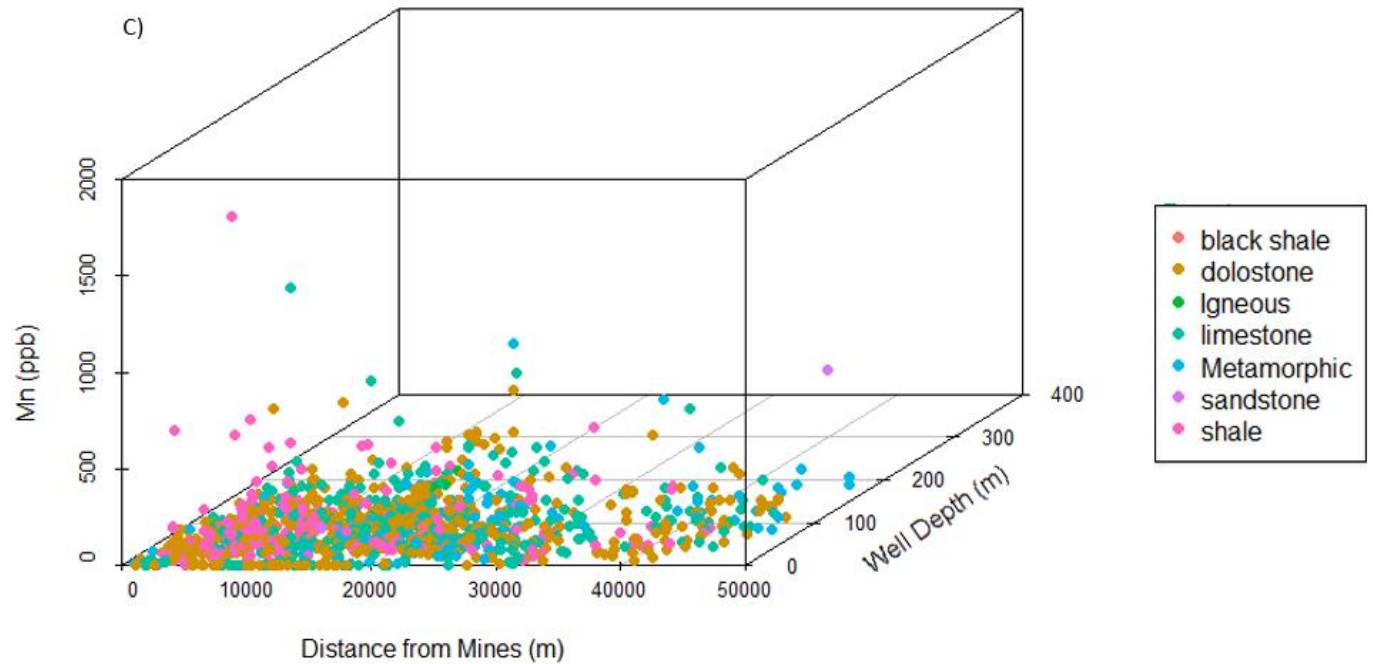
**Figure 5:** 3D scatterplot series depicting $Mn^{2+}$ concentrations (ppb), well depth (m), and distance in meters from A) surface water; B) geologic structure including faults, dikes, and sills; and C) historic Mn mines.

To gain more insight into the possible controls on elevated $Mn^{2+}$ in groundwater, I calculated the distance between well locations and potential explanatory variables (surface water, geologic structure, and mines) to compare the distance between wells and these features simultaneously with $Mn^{2+}$ concentration and well depth (Figure 5); all samples are categorized by host lithology. Figure 5A depicts distance from surface water: samples with elevated $Mn^{2+}$ are generally located in closer proximity to surface water, and $Mn^{2+}$ concentrations decrease with distance. Due to the dense distribution of surface waters in the valley (Figure 4A), the vast majority of samples are within 1000 m of surface water. As observed in Figure 2E, most samples with elevated $Mn^{2+}$ are located within shale lithologies within ~150 m of the surface. Figure 5B depicts distance from geologic structure (faults, dikes, and sills), while Figure 5C depicts distance from Mn mines. In both figures, samples are fairly evenly distributed with distance from geologic structures and

mines, respectively. This suggests that proximity to structures and mines does not exhibit significant control over groundwater $Mn^{2+}$ concentrations.

**Statistical analyses**

Multivariate statistical analyses were used to identify chemical processes that are difficult to elucidate with individual bivariate analyses. Figure 6 depicts results from the HCA. Shown are the relationships between 25 analytes from 1488 groundwater samples within the dataset. A HCA was also performed with 986 samples across 31 analytes, available in Appendix A. Importantly, whether the HCA was performed with more samples with fewer analytes or fewer samples with more analytes, the interpretation of chemical processes did not change. There are four predominant analyte clusters (from left to right): 1) trace metals (Cr, Ni, Pb, V, Mo, F, Sn, As, Co, Ag, Cd,) 2) Al, Fe, and Mn: Mn clusters with Fe (redox-controlled) and co-occurs with Al, 3) $NO_3$, Si, P, Cu, and Zn 4) analytes associated with a) water hardness or b) the application of a water softener system which treats hardness through ion exchange ($K^+$, Hardness, $Mg^{2+}$, $Ca^{2+}$, $Na^+$, $SO_4^{2-}$). Water hardness components include $Ca^{2+}$, $Mg^{2+}$, and (to a minor extent) $SO_4^{2-}$; water softeners utilize salts containing $Na^+$ and $K^+$ to reduce water hardness, thus samples containing elevated concentrations of these analytes are indicative of treated water.
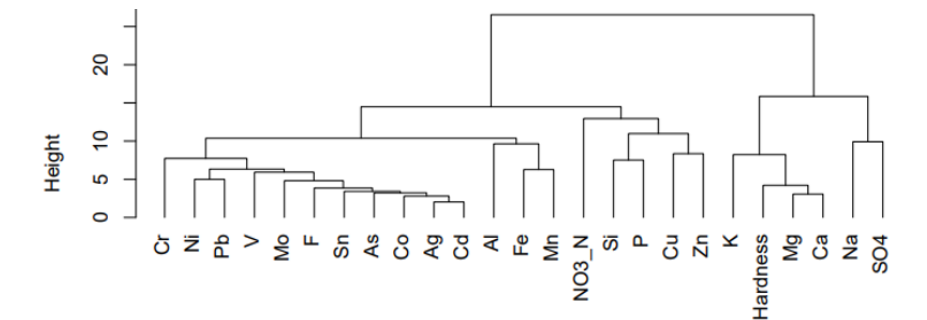


**Figure 6:** Results of a hierarchical cluster analysis (HCA) of 1488 samples across 25 analytes. Four analyte clusters are apparent (from left to right): 1) trace metals; 2) redox-controlled analytes; 3) $NO_3$, Si, P, Cu, and Zn; and 4) analytes associated with water hardness.

A PCA biplot depicts the data from 1488 samples across 25 analytes (Figure 7). An alternate PCA was generated with 985 samples across 31 analytes (Appendix B), though it ultimately exhibits the same general vector relationships and geochemical interpretations. $Ca^{2+}$, $Mg^{2+}$, and Hardness plot as elongated, tightly-clustered vectors in the direction of positive principal component 1 (PC1) space. Additionally, other divalent trace ions such as $Sr^{2+}$ and $Ba^{2+}$ exert an influence on PC1 in the positive direction, ultimately plotting along with $Ca^{2+}$, $Mg^{2+}$, and Hardness. In contrast, the $Na^+$ vector points in the opposite direction, into negative PC1 space. No other analytes associate strongly with $Na^+$ in PC1 space. Thus, PC1 is defined as water treatment status: untreated samples fall in positive PC1 space, while treated samples fall in negative PC1 space and have undergone water softening such that they are left only with significant amounts of $Na^+$, a component in water softening salts. There is no clear separation of samples by lithology along the PC1 axis; while metamorphic samples tend to fall disproportionately in positive PC1 space, all other lithologies are equally prevalent across the PC1 axis. This reinforces the notion that PC1 is water treatment status; whether or not a sample has been treated is completely independent of host lithology.
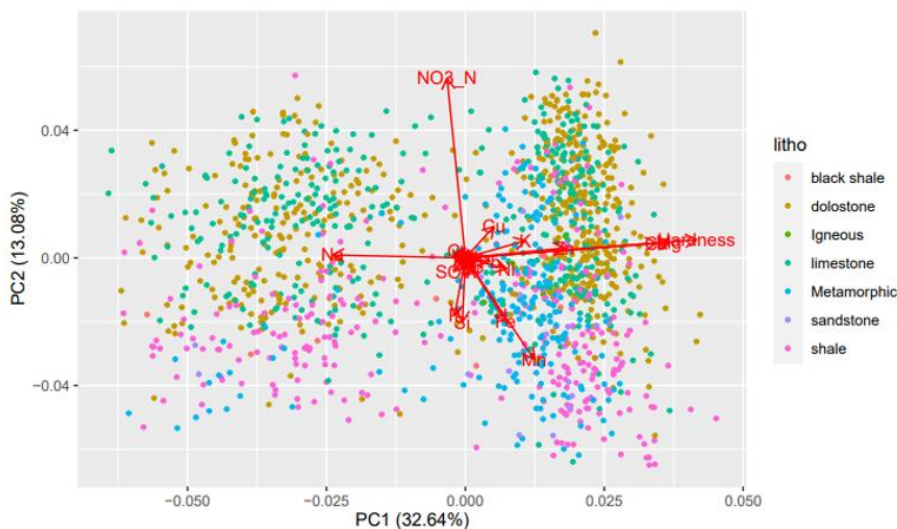


**Figure 7:** Results of a principal component analysis (PCA) of 1488 samples across 25 analytes.

The $NO_3\_N$ vector exerts control on principal component 2 (PC2) in the positive dimension and is juxtaposed with Mn and Fe, which are tightly coupled and exert the most control in the negative PC2 dimension. Additionally, Si and P exert control in the negative PC2 dimension, though to a lesser extent than Mn and Fe. Separation by lithology is more prevalent in PC2 than in PC1. While carbonates occur in both positive and negative PC2 space, they occur more frequently in positive PC2 space. In contrast, shales are far more abundant in negative PC2 space. Thus, I interpret PC2 is indicative of redox conditions; positive PC2 space reflects oxidizing conditions while negative PC2 space reflects reducing conditions.

Most trace metals do not heavily influence either PC1 or PC2, as indicated by short vectors. However, they trend toward positive PC1 space and negative PC2 space: this is indicative of untreated samples under reducing conditions.

## DISCUSSION

### Effect of home water treatments

During VAHWQP data collection, a questionnaire was issued to property owners concerning factors that may influence water testing results. One component of the questionnaire dealt with which water treatment methods, if any, were in place at the testing site. Possible water treatment methods included the following: acid neutralizer, ultraviolet light, water softener, sediment filter, reverse osmosis, iron removal, carbon filter, and chlorinator. Of these possible treatments, the presence of a water softener likely exhibited the greatest influence on water testing results. Water softeners operate by replacing $Ca^{2+}$ and $Mg^{2+}$ ions (components of hard water) with $Na^+$ ions. This process is evident in Figure 7, where there is a strong dichotomy along the PC1 axis with the $Na^+$ vector pointing into negative PC1 space and all other analytes, including the cluster

of vectors related to hard water ($Ca^{2+}$, $Mg^{2+}$, Hardness, $Sr^{2+}$, $Ba^{2+}$), pointing into positive PC1 space. The principal component analysis brings to light the effectiveness of the treatment process, as hundreds of samples from limestone and dolostone aquifers associate with the $Na^+$ vector and opposite of the $Ca^{2+}$ and $Mg^{2+}$ vectors, suggesting that $Ca^{2+}$ and $Mg^{2+}$ in the native groundwater have been effectively exchanged for $Na^+$ during the water softening process. From this, we interpret that the variable that controls the most variance in our dataset is not geologically related whatsoever, but rather a consequence of water treatment, where treated samples fall into negative PC1 space and untreated samples fall into positive PC1 space. This has multiple implications for assessing water quality in this study. First, treated samples are not truly reflective of the groundwater at that location, which may confound geochemical interpretations. In fact, elemental correlations might markedly increase if treated samples are removed from dataset. Second, the exchange reaction of $Na^+$ for $Ca^{2+}$ and $Mg^{2+}$ likely also occurs for $Mn^{2+}$ if it is also present in groundwater. Because $Mn^{2+}$ has a smaller ionic radius (91 pm) than $Ca^{2+}$ (231 pm) and $Mg^{2+}$ (173 pm), but it has the same valence, it is a more charge-dense ion, making it more likely to participate in exchange reactions during water softening. Therefore, a treatment system that removes $Ca^{2+}$ and $Mg^{2+}$ likely also removes some, if not most $Mn^{2+}$.

**Anthropogenic sources of Mn**

In Figure 5B and 5C, samples are fairly evenly distributed with distance from geologic structures and mines, respectively, implying that the combined factors of depth with distance from geologic structure and mines do not influence groundwater $Mn^{2+}$ concentrations. However, it is clear that $Mn^{2+}$ concentrations generally decrease with depth (Figure 2E). While historic Mn mines (Figure 4E) reflect the presence of Mn ores, their existence does not seem to influence groundwater $Mn^{2+}$ concentrations in the vicinity of mines, even in samples located down a steep slope from a

mine. Orchards are sparsely distributed near the valley's eastern margin. Given the lack of orchards in proximity to samples with elevated Mn, their existence does not seem to influence groundwater $Mn^{2+}$ concentrations.

For the TOP/BOT ratio, Mn soil concentrations in the C horizon remain fairly constant throughout the valley, while Mn concentrations in topsoil gradually increase toward the northern end of the valley. Higher Mn topsoil concentrations may be the result of anthropogenic inputs: both engine exhaust along roadways and application of Mn-containing fungicides Maneb® and Mancozeb® in orchards can deposit Mn in the topsoil. However, both roadways and orchards are fairly evenly distributed with latitude throughout the valley, so this does not explain observed higher Mn topsoil concentrations in the northern portion of the valley. A more likely culprit is mechanical weathering of soils. This involves the weathering and erosion of Mn-bearing minerals along steep slopes that then accumulate as Mn oxides in shallow slopes that flank the Massanutten Mountain Range in the valley center (note the steep slope in the mid-latitudes of the valley center in Figure 4D). While this range is present in the middle (2 - 4) and high (>4) TOP/BOT regions, it is completely absent from the low (< 2) TOP/BOT region in the valley's southern end. Steeper slopes cause faster runoff velocities, thus more free energy is available for both physical soil weathering and transport of chemically-weathered products. One serious limitation of TOP/BOT analysis is that it assumes both soil samples at depth (BOT) and topsoil (TOP) are undergoing the same geogenic processes, and elevated concentrations in TOP must be the result of anthropogenic input (Reimann, 2008). However, a TOP/BOT analysis is still useful in that it illuminates a discrepancy between TOP and BOT concentrations as long as geogenic explanations are considered in addition to anthropogenic ones. In fact, we propose in our conceptual model (below)

that some geologic processes can deliver $Mn^{2+}$ from depth to the topsoil while circumnavigating the deeper soil horizons altogether.

**Geogenic sources of $Mn^{2+}$ in groundwater**

As observed in a geospatial (Figure 4B) and statistical (Table 2) context, the majority of elevated groundwater $Mn^{2+}$ samples occur in a shale host lithology. However, samples in sandstone and metamorphic lithologies may also feature high Mn. An analysis of the PC2 axis in Figure 6 suggests it is reflective of redox conditions: negative PC2 space reflects reducing conditions and subsequent mobilization of metals such as $Mn^{2+}$ and $Fe^{2+}$, while positive PC2 space reflects oxidizing conditions and is most heavily influenced by the $NO_3$_N vector. Generally, most sandstone and shale groundwater samples plot in the negative PC2 space, indicating they are in reducing conditions.

The juxtaposition between $NO_3^-$ and the $Fe^{2+}/Mn^{2+}$ cluster occurs because $NO_3^-$ occurs in oxic-to sub-oxic waters and is most commonly sourced from agricultural fertilizer, suggesting that $NO_3^-$-rich waters have a direct and recent connection with the surface. $NO_3^-$ can also poise an aquifer's redox state to relatively high Eh by coupling biodegradation to $NO_3$-reduction. While biodegradation is most thermodynamically favored when coupled to DO, DO is relatively insoluble in cold water and reaches 100% saturation at 9-11 mg/L for most groundwater, so it is often rapidly consumed by microbial activity, giving way to anaerobic biodegradation coupled to Mn- and Fe-reduction. However, $NO_3^-$ can inhibit the onset of anoxia. Unlike DO, $NO_3^-$, can accumulate to tens to hundreds of mg/L, thus permitting biodegradation to occur at an Eh higher than if $NO_3^-$ were absent for greater periods of time. In other words, $NO_3^-$ provides a buffer to the onset of Mn-reducing conditions. Additionally, $Fe^{2+}$ and $Mn^{2+}$ cluster tightly in the HCA (Figure 6), suggesting they are mobilized together due to reductive dissolution in anoxic conditions. High

organic content in shales tends to consume dissolved oxygen during decay, thus generating reducing conditions. This phenomenon is reinforced by the fact that the majority of samples with shale host lithology plot in negative PC2 space, which is reflective of anoxic conditions. Additionally, $Mn^{2+}$ and As plot together in PC2 space (additionally, r = 0.753 for $Mn^{2+}$ and As in shale lithologies, Table 2): this reflects the ability of Mn oxides to sorb As, thus co-contamination of both $Mn^{2+}$ and As occurs with the reductive dissolution of Mn oxides.

**Conceptual model**

Figures 4A and 5A reflect how elevated $Mn^{2+}$ concentrations in groundwater are located closer to surface waters such as rivers. Two alternate models may explain this distribution: recharge and discharge. A recharge or a "top down" model involves the delivery of organic matter in surface water to nearby soils and sediments via flooding events, during which organic-rich sediments are deposited on the floodplain and accumulate in soils (Gillispie et al., 2016). Organic matter is an electron donor for microorganisms, which allows them to rapidly deplete dissolved oxygen (DO) from recharging water and contributes to anoxic conditions and facilitates the reductive dissolution of Mn oxides. This model has been used to explain elevated As and Fe in groundwater in southeast Asia (Polizzotto et al., 2008). Under this model, high $Mn^{2+}$ concentrations would be expected in shallow groundwater and would increase with depth along recharge flow paths as groundwater became more reducing and releases more Mn. In this study, $Mn^{2+}$ concentrations vs depth data show the opposite trend (Figure 2E), making this model unlikely.

An alternative discharge, or "bottom up", model could also explain elevated $Mn^{2+}$ near rivers, particularly in the center of the valley. In this model, groundwater recharge enters the

27

subsurface along the valley margins, and groundwater age increases along long flow paths as it flows toward the discharge point in the valley center (i.e., major river systems). More favorable electron acceptors ($O_2$, $NO_3$) are consumed along the flow path, contributing to increasingly anoxic conditions as the water ages. When old, anoxic groundwater discharges near major river systems in the valley's center, it reductively dissolves Mn oxides into groundwater and allows $Mn^{2+}$ to contaminate wells in the vicinity. Under this model, one would expect that groundwater $Mn^{2+}$ concentrations would be low at depth, prior to the onset of Mn-reducing conditions. But as water begins to discharge upward, $Mn^{2+}$ concentrations would increase as groundwater ages and becomes more reducing near the surface, which can be observed in Figure 2E. This phenomenon would be exacerbated by the presence of rocks containing ample organic carbon like the shales in the north-central part of the Shenandoah Valley. This likely explains why zones of elevated $Mn^{2+}$ occur in the valley center.
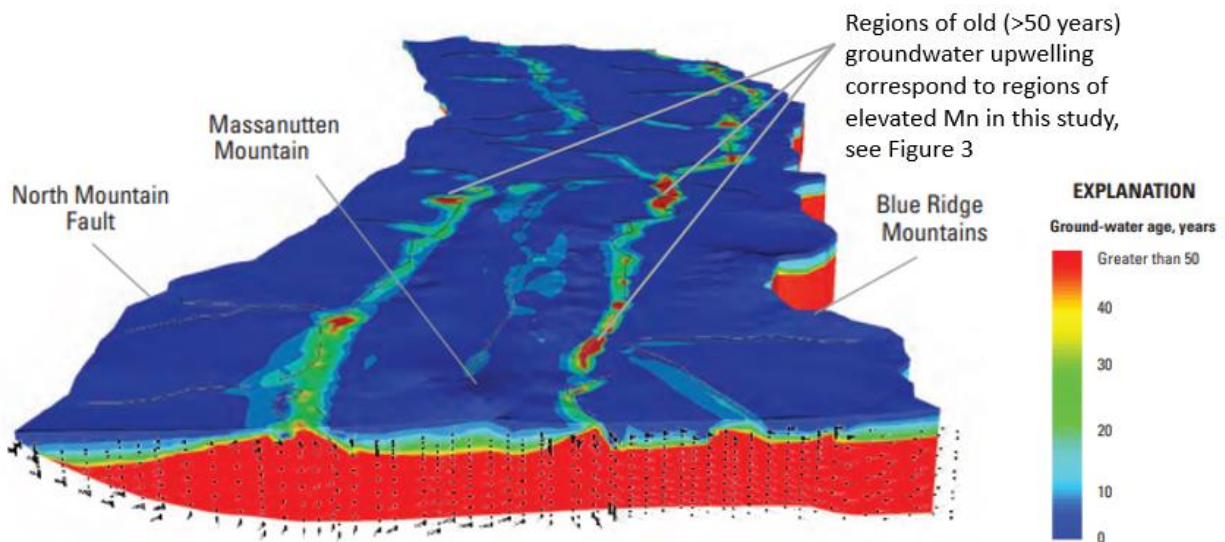


**Figure 8:** Groundwater flow and age modeling, modified from Yager et al. (2009).

The bottom-up model is supported by previous hydrogeologic modeling by Yager et al. (2009) (Figure 8), which evinces regions of old, anoxic groundwater upwelling along rivers. These regions of upwelling coincide with the clusters of elevated $Mn^{2+}$ samples (Figure 3), thus supporting the bottom-up model. As observed in Figure 8, upwelling groundwater along rivers ranges from 50 – 20 years old, which is significantly older than the majority of near-surface groundwater in the valley that is <10 years in age.

**Chemical weathering in shales**

Mineralogical constituents of the Martinsburg Formation include quartz, phyllosilicates (muscovite, chlorite), sulfides (pyrite, chalcopyrite, galena, sphalerite), and carbonaceous material (Feldman et al. 2009; McBride 1962). Shale is the primary lithologic constituent of the Martinsburg Formation, sandstone and siltstone are minor constituents, while limestone is an incidental constituent. As observed in Figure 2G, $SO_4^{2-}$ concentrations are elevated across many samples and especially those with a shale host lithology. Given the presence of sulfides in the Martinsburg, oxidation of these sulfide minerals is likely a major contributing factor to elevated $SO_4^{2-}$ concentrations. Conversely, sulfide oxidation consumes $O_2$, thus further contributing to anoxic conditions that facilitate the reductive dissolution of Mn oxides. As observed in Figures 2C and 2F, $Ca^{2+}$ and $Mg^{2+}$ concentrations are elevated across many samples, especially those with shale host lithologies. The weathering of phyllosilicates within the Martinsburg via hydrolysis may mobilize $Ca^{2+}$ and $Mg^{2+}$, thus accounting for elevated concentrations of these analytes in tandem with $Mn^{2+}$ in shales.

**Formation of Mn oxides**

It is clear from the HCA (Figure 6) and PCA (Figure 7) that reducing conditions, and thus microbial reduction of Mn oxides, is responsible for elevated $Mn^{2+}$ in groundwater in shales of the Shenandoah Valley. However, the geochemical explanation for the presence of Mn oxides in shale deposits requires further investigation. Because shales form under reducing conditions, Mn oxides are not likely formed as part of the primary mineral assemblage during deposition. Instead, the presence of Mn oxides is more likely a consequence of more recent elemental cycling.

As observed in Figure 8, groundwater recharges at the valley's margins and flows toward the center, where it upwells along river channels. Along this flow path from the valley margins to the center, groundwater encounters carbonate lithologies, which can also have elevated $Mn^{2+}$ (Table 3). Force and Cox (1991) identified supergene Mn deposits in carbonates rocks in the Shenandoah Valley as the primary source of historically-mined Mn ore, and Hack (1965) proposed that carbonates (and any Mn contained in the solid solution lattice) dissolve when exposed to acidic rainwater with a pH of 5.0-6.5 and later precipitate out of solution as Mn oxides in the center of the valley with the discharge of higher pH (>7)groundwater. Furthermore, Kiracofe et al. (2017) identifies carbonate lithologies as the primary source of aqueous $Mn^{2+}$ in the Roanoke River Watershed of Southern Virginia.

One possible explanation for the formation of Mn oxides in the Martinsburg near the valley's center is that groundwater reductively dissolves supergene Mn ore deposits in carbonate lithologies as it flows toward the valley center as previously observed by Force and Cox (1991). When it upwells at the valley center, anoxic, $Mn^{2+}$ enriched groundwater encounters more oxygenated stream water that diffuses into aquifer sediments adjacent to the stream channel, thus

forming Mn oxides. These Mn oxides, which form due to shorter, shallower flow paths, are then able to be dissolved when old anoxic groundwater from deep flow paths discharges upward and reduces the recently formed Mn oxides at the valley's center, resulting in elevated $Mn^{2+}$ concentrations in groundwater near stream channels. This process is illustrated in Figure 9.
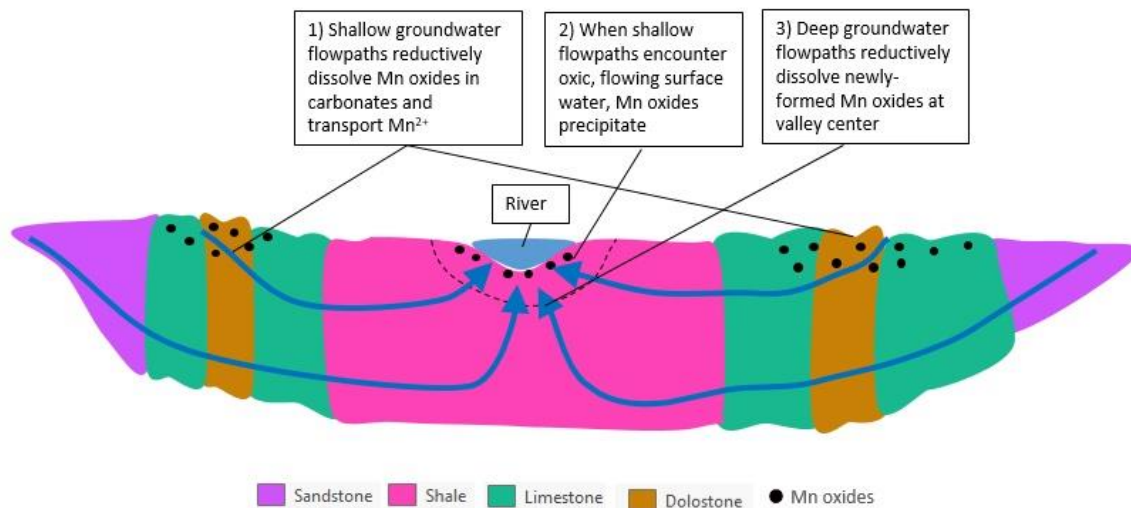


**Figure 9:** A possible explanation for the reallocation of $Mn^{2+}$ from carbonate to shale lithologies via groundwater flow.
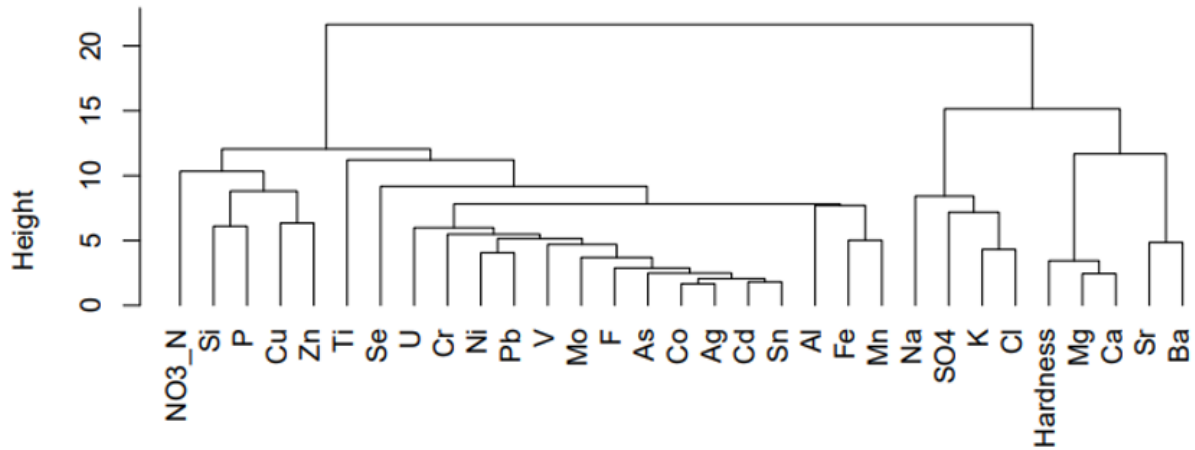
## CONCLUSIONS

This study sought to identify primary mechanisms of $Mn^{2+}$ introduction into groundwater in the Shenandoah Valley of Virginia. While soil weathering and anthropogenic input hypotheses were also considered, this study concludes that a combination of redox conditions, groundwater flow paths, and host lithology is the primary culprit of elevated $Mn^{2+}$ in select areas within the Shenandoah Valley. Elevated $Mn^{2+}$ samples are located primarily in shale host lithologies, which are associated with reducing conditions that reductively dissolve previously existing Mn oxides to mobilize $Mn^{2+}$ to groundwater in the vicinity. Overall, those who source drinking water from wells

in the Shenandoah Valley should be cautious of consuming untreated water within shale lithologies. Future work will involve the isolation of only untreated samples from the VAHWQP dataset.
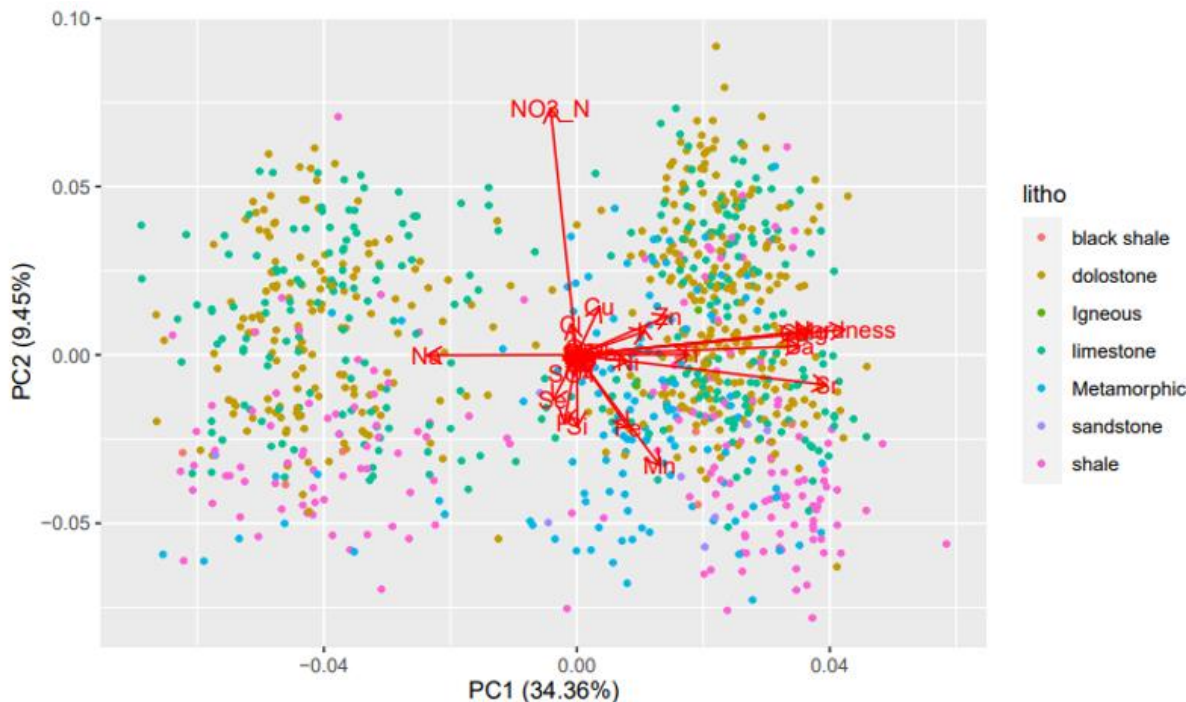
## ACKNOWLEDGEMENTS

**Appendix A**

**Appendix B**



# REFERENCES

Bjørklund, G., Chartrand, M.S., and Aaseth, J., 2017, Manganese exposure and neurotoxic effects in children: Environmental Research, v. 155, p. 380–384, doi:10.1016/j.envres.2017.03.003.

Bouchard, M., Laforest, F., Vandelac, L., Bellinger, D., and Mergler, D., 2007, Hair Manganese and Hyperactive Behaviors: Pilot Study of School-Age Children Exposed through Tap Water: Environmental Health Perspectives, v. 115, p. 122–127, doi:10.1289/ehp.9504.

Bouchard, M.F., Sauvé, S., Barbeau, B., Legrand, M., Brodeur, M.-È., Bouffard, T., Limoges, E., Bellinger, D.C., and Mergler, D., 2011, Intellectual Impairment in School-Age Children Exposed to Manganese from Drinking Water: Environmental Health Perspectives, v. 119, p. 138–143, doi:10.1289/ehp.1002321.

Di-Ruggiero, J., and A. M. Gounot. "Microbial manganese reduction mediated by bacterial strains isolated from aquifer sediments." *Microbial ecology* 20.1 (1990): 53-63.

Feldman, H., Epstein, J., & Smoliga, J.(2009). The Shawangunk and Martinsburg Formations revisited; sedimentology, stratigraphy, mineralogy, geochemistry, structure and paleontology. New York State Geological Association 81st annual meeting; field trip guidebook, Vol. 81, p.12.

Force, E. R., & Cox, L. J, 1991. Manganese contents of some sedimentary rocks of Paleozoic Age in Virginia / by Eric R. Force and Leslie J. Cox.

Gillispie, E.C., Austin, R.E., Rivera, N.A., Bolich, R., Duckworth, O.W., Bradley, P., Amoozegar, A., Hesterberg, D., and Polizzotto, M.L., 2016, Soil Weathering as an Engine for Manganese Contamination of Well Water: Environmental Science & Technology, v. 50, p. 9963–9971, doi:10.1021/acs.est.6b01686.

Hack, J.T (n.d.) (1965), Geomorphology of the Shenandoah Valley Virginia and West Virginia and Origin of the Residual Ore Deposits. United States Department of the Interior

Hafeman, D., Factor-Litvak, P., Cheng, Z., van Geen, A., and Ahsan, H., 2007, Association between Manganese Exposure through Drinking Water and Infant Mortality in Bangladesh: Environmental Health Perspectives, v. 115, p. 1107–1112, doi:10.1289/ehp.10051.

Hotelling H. Analysis of a complex of statistical variables into principal components. *Journal of Educational Psychology*, 24:417–441, 1933.

Hue, N. V.; Vega, S.; Silva, J. A. Manganese Toxicity in a Hawaiian Oxisol Affected by Soil PH and Organic Amendments. *Soil Science Society of America Journal* **2001**, *65* (1), 153–160. https://doi.org/10.2136/sssaj2001.651153x.

Hue, N.V., Vega, S., Silva, J.A., 2001. Manganese Toxicity in a Hawaiian Oxisol Affected by Soil pH and Organic Amendments. Soil Sci. Soc. Am. J. 65, 153–160. https://doi.org/10.2136/sssaj2001.651153x

Kaufman L. and Rousseeuw P.J. *Finding Groups in Data*. John Wiley & Sons, Inc., New York, 1990.

Khan, K. et al., 2012, Manganese exposure from drinking water and children's academic achievement: NeuroToxicology, v. 33, p. 91–97, doi:10.1016/j.neuro.2011.12.002.

Langley, R., Kao, Y., Mort, S., Bateman, A., Simpson, B., and Reich, B., 2015, Adverse neurodevelopmental effects and hearing loss in children associated with manganese in well water, North Carolina, USA: Journal of Environmental and Occupational Science, v. 4, p. 62, doi:10.5455/jeos.20150403060427.

Li, M.S., Luo, Y.P., Su, Z.Y., 2007. Heavy metal concentrations in soils and plant accumulation in a restored manganese mineland in Guangxi, South China. Environmental Pollution 147, 168–175. https://doi.org/10.1016/j.envpol.2006.08.006

Ljung, K., and Vahter, M., 2007, Time to Re-evaluate the Guideline Value for Manganese in Drinking Water? Environmental Health Perspectives, v. 115, p. 1533–1538, doi:10.1289/ehp.10316.

Lytle, C. M.; Smith, B. N.; McKinnon, C. Z. Manganese Accumulation along Utah Roadways: A Possible Indication of Motor Vehicle Exhaust Pollution. *Science of The Total Environment* **1995**, *162* (2), 105–109. https://doi.org/10.1016/0048-9697(95)04438-7.

Mcbride, E. F, 1962. Flysch and Associated Beds of the Martinsburg Formation (Ordovician), Central Appalachians. In Journal of Sedimentary (Vol. 32, Issue 1). http://pubs.geoscienceworld.org/sepm/jsedres/article-pdf/32/1/39/2803324/39.pdf

McMahon, P.B., Belitz, K., Reddy, J.E., and Johnson, T.D., 2018, Elevated Manganese Concentrations in United States Groundwater, Role of Land Surface–Soil–Aquifer Connections: Environmental Science & Technology, v. 53, p. 29–38.

Mendenhall, W. C., & Monroe, W. H., 1942. United States Department of the Interior Harold L. Ickes, Secretary Geological Survey Manganese Deposits of the Cedar Creek Valley, Frederick and Shenandoah Counties, Virginia Strategic Minerals Investigations, (Pages 111-141) United States Government Printing Office.

Polizzotto, M., Kocar, B., Benner, S. *et al.* Near-surface wetland sediments as a source of arsenic release to ground water in Asia. *Nature* **454,** 505–508 (2008). https://doi.org/10.1038/nature07093

Reimann, C. , 2008. Statistical data analysis explained : applied environmental statistics with R. John Wiley & Sons.

Sanders, A.P., Desrosiers, T.A., Warren, J.L., Herring, A.H., Enright, D., Olshan, A.F., Meyer, R.E., and Fry, R.C., 2014, Association between arsenic, cadmium, manganese, and lead levels in private wells and birth defects prevalence in North Carolina: a semi-ecologic study: BMC Public Health, v. 14, p. 955, doi:10.1186/1471-2458-14-955.

Semu, E., Singh, B.R., 1995. Accumulation of heavy metals in soils and plants after long-term use of fertilizers and fungicides in Tanzania. Fertilizer research 44, 241–248. https://doi.org/10.1007/BF00750931

Shapiro, S.S. and Wilk, M.B. (1965). An analysis of variance test for normality (complete samples). *Biometrika* **52**: 591-611.

Spangler, A.H., and Spangler, J.G., 2009, Groundwater Manganese and Infant Mortality Rate by County in North Carolina: An Ecological Analysis: EcoHealth, v. 6, p. 596–600, doi:10.1007/s10393-010-0291-4.

Spangler, J.G., and Reid, J.C., 2010, Environmental Manganese and Cancer Mortality Rates by County in North Carolina: An Ecological Study: Biological Trace Element Research, v. 133, p. 128–135, doi:10.1007/s12011-009-8415-9.

U.S. Census Bureau, 2019, Population of Virginia by County.

U.S. Environmental Protection Agency, 2004, Drinking Water Health Advisory for Manganese.

Virginia State Water Resources Plan, 2015.

Wehr, F., 1985. Stratigraphy and tectonics of the Virginia-North Carolina Blue Ridge: Evolution of a late Proterozoic-early Paleozoic hinge zone. http://pubs.geoscienceworld.org/gsa/gsabulletin/article-pdf/96/3/285/3434398/i0016-7606-96-3-285.pdf

Yager, R.M., Voss, C.I., and Southworth, S., 2009, Comparison of alternative representations of hydraulic-conductivity anisotropy in folded fractured-sedimentary rock: modeling groundwater flow in the Shenandoah Valley (USA): Hydrogeology Journal, v. 17, p. 1111–1131, doi:10.1007/s10040-008-0431-x.